remote sensing

MDPI

Article

Classification of Geomorphic Units and Their Relevance for Nutrient Retention or Export of a Large Lowland Padma River, Bangladesh: A NDVI Based Approach

Md Ataul Gani [1,2,3,*], Johannes van der Kwast [4], Michael E. McClain [1,5], Gretchen Gettel [1] and Kenneth Irvine [1,2]

[1] Department of Water Resources and Ecosystems, IHE Delft Institute for Water Education, P.O. Box 3015, 2601 DA Delft, The Netherlands; m.mcclain@un-ihe.org (M.E.M.); g.gettel@un-ihe.org (G.G.); k.irvine@un-ihe.org (K.I.)
[2] Aquatic Ecology and Water Quality Management Group, Department of Environmental Sciences, Wageningen University and Research, P.O. Box 47, 6700 AA Wageningen, The Netherlands
[3] Department of Botany, Jagannath University, Dhaka 1100, Bangladesh
[4] Department of Land and Water Management, IHE Delft Institute for Water Education, P.O. Box 3015, 2601 DA Delft, The Netherlands; h.vanderkwast@un-ihe.org
[5] Department of Water Management, Delft University of Technology, P.O. Box 5048, 2600 GA Delft, The Netherlands
* Correspondence: m.gani@un-ihe.org

Abstract: Geomorphic classification of large rivers identifies morphological patterns, as a foundation for estimating biogeochemical and ecological processes. In order to support the modelling of in-channel nutrient retention or export, the classification of geomorphic units (GUs) was done in the Padma River, Bangladesh, a large and geomorphically-complex lowland river. GUs were classified using the normalized difference vegetation index (NDVI) four times over a year, so as to cover the seasonal variation of water flows. GUs were categorized as primary and secondary channels (C & S); longitudinal bar (L); transverse bar (T); side bar (SB); unvegetated bank (EK); dry channel (ED); island (VI); and water depression (WD). All types of GUs were observed over the four distinct annual seasons, except ED, which was absent during the high flow, monsoon season. Seasonal variation of the surface area of GUs and discharge showed an inverse relation between discharge and exposed surface areas of VI, L, T, and SB. Nutrients mainly enter the river system through water and sediments, and during monsoon, the maximum portion of emergent GUs were submerged. Based on the assumption that nutrient retention is enhanced in the seasonally inundated portions of GUs, nutrient retention-/export-relevant geomorphic units (NREGUs) were identified. Seasonal variation in the area of NREGUs was similar to that of GUs. The mean NDVI values of the main identified NREGUs were different. The variation of NDVI values among seasons in these NREGUs resulted from changes of vegetation cover and type. The variation also occurred due to alteration of the surface area of GUs in different seasons. The changes of vegetation cover indicated by NDVI values across seasons are likely important drivers for biogeochemical and ecological processes.

Keywords: geomorphic classification; geomorphic units; NDVI; Sentinel 2; QGIS; nutrient retention/export; large lowland river; Padma River; Bangladesh

Citation: Gani, M.A.; Kwast, J.v.d.; McClain, M.E.; Gettel, G.; Irvine, K. Classification of Geomorphic Units and Their Relevance for Nutrient Retention or Export of a Large Lowland Padma River, Bangladesh: A NDVI Based Approach. *Remote Sens.* **2022**, *14*, 1481. https://doi.org/10.3390/rs14061481

Academic Editor: Jerry D Davis

Received: 27 January 2022
Accepted: 16 March 2022
Published: 18 March 2022

1. Introduction

River biodiversity and ecosystem functioning depend on the geomorphology and erosional and depositional processes within geomorphic units [1,2]. Geomorphic units, hereafter GUs, are discrete morphodynamic entities, considered building blocks of the river and defined by their position, morphology, and sediment composition. Generally, GUs are mapped at reach scale, because this scale is important for hydromorphological factors, such as water flow and sediment transport [3]. Different classification schemes have been

proposed to delineate and map GUs at the scale of the river reach. Wyrick and Pasternack [4] classified GUs based on hydraulic data (flow velocity and depth), whereas Wheaton et al. [5] classified GUs based on topographic and morphological characteristics (position, attributes of sediment and vegetation). Classification of GUs has been developed to cover a wide range of river types (lowland systems, mountain systems, highly dynamic systems, etc.) and includes different sub-domains (vegetation, bed configuration, sedimentary units) and scales (macro-unit, unit, and sub-unit) [3,6].

Nutrient retention or export is influenced by seasonal discharge [7,8] and biogeochemical processes [9–11]. Nutrients in a river channel are both taken up by, and released from, the river bed. Data for large rivers have shown the primary importance of discharge for nutrient flux [12,13]. Morphological changes in large rivers influence nutrient removal processes and loads to the deltas or downstream water bodies. With climate change, the water volume and seasonal flow of some of the world's biggest rivers are projected to change markedly [14], changing sediment mobility and ecological functioning [13]. The sediment load to large river systems reshapes channel morphology [15], with consequences for biogeochemical processes and in-stream nutrient retention [16]. GUs can be inundated temporally and enriched with nutrients. This is usually observed in floodplain areas and riparian zones. Plant uptake and denitrification are biogeochemical processes that contribute to nitrogen removal from riparian wetlands [17,18]. Vegetation influences these processes, by both taking up nutrients directly and influencing subsurface denitrification in their root zones [19].

A variety of satellite imagery is available for monitoring inland water quality and issues related to nutrient retention, such as water transparency, eutrophication, organic matter, biomass estimation, nutrient, and chlorophyll concentration [20–27]. Recently, satellite-derived estimates of flood and vegetation cover are increasingly used in monitoring [28–31]. However, this has not gone as far as estimating biogeochemical processes [32] or nutrient retention as a function of vegetation cover [33], although land use and land cover (LULC) maps are frequently generated using satellites [34–37].

In comparison with the commonly used, and previous, SPOT and Landsat products of satellites, the new generations of freely available satellite imagery provide high-resolution multispectral imaging, with a high revisit frequency for the detection of temporal changes in LULC, including inland waters [38,39]. Sentinel-2, with 13 spectral bands, can be used to derive biogeophysical indices that combine different band reflectances. This allows for calculations of the normalized difference water index (NDWI, [40]), which separates water cover from land surfaces [41], and the enhanced vegetation index (EVI, [42]), which corrects soil background signals and atmospheric influences, to identify forest/canopy cover, enhancing estimates of the well-known normalized difference vegetation index (NDVI, [43]) that is often used for separating soil, water, and vegetation classes [44]. In-channel GUs consist of water, sediment, and vegetation [45–47]. Nutrient retention processes in GUs are related to biophysical activities and water availability [48–50]. One of the advantages of NDVI is that it can be used to monitor the biophysical conditions related to natural water retention [51–53] and that it is sensitive to low vegetation cover [41]. However, there is a debate over EVI, regarding illumination conditions and hydroclimatic factors at decadal scales [54,55]. Nevertheless, characteristic local features need to be considered in the estimation of biophysical indices [56].

NDVI has been used for monitoring the vegetation and ecosystem dynamics of large rivers [57–61]. Relationships between seasonal vegetation and discharge variation of large rivers can be verified by the seasonal correlation between NDVI and discharge [62]. In the Parana River of South America, NDVI was used to assess fluvial dynamics, describe ecological patterns [57], and establish a relation between vegetation and GUs [59]. The latter has brought an opportunity to utilize NDVI to classify GUs in large lowland rivers.

Different classification schemes of GUs have been presented, but none focus on the seasonal variation of GUs, except Marchetti et al. [59], who used NDVI to show only the dynamics of floodplain vegetation GUs. In this paper, we set out to develop an NDVI-

based geomorphic classification scheme for a large lowland river that reflects its relevance for nutrient retention and export. Therefore, the objectives of the present study are to (i) classify GUs considering the seasonal variation of a large lowland river based on remote sensing data, (ii) map areas of GUs assumed to be important for nutrient retention or export, (iii) show the seasonal dynamics of GUs, focusing on nutrient retention and export and, (iv) demonstrate the effectiveness of NDVI and shape indexes for the present classification.

2. Materials and Methods

2.1. Study Area

The study area is a part of the Padma River, downstream of the confluence of the Ganges and Brahmaputra rivers (Figure 1). The morphology of the Padma River is highly variable, ranging from straight, to meandering and braided channels [63]. The erosion and deposition patterns of the river reshape the islands and bars (locally called *chars*) [64], which range from 1 to 36 years in age. Some are occupied by human settlements [65]. Naturally, islands are a vegetated portion of the study area, but the edges are bare land that is inundated seasonally.

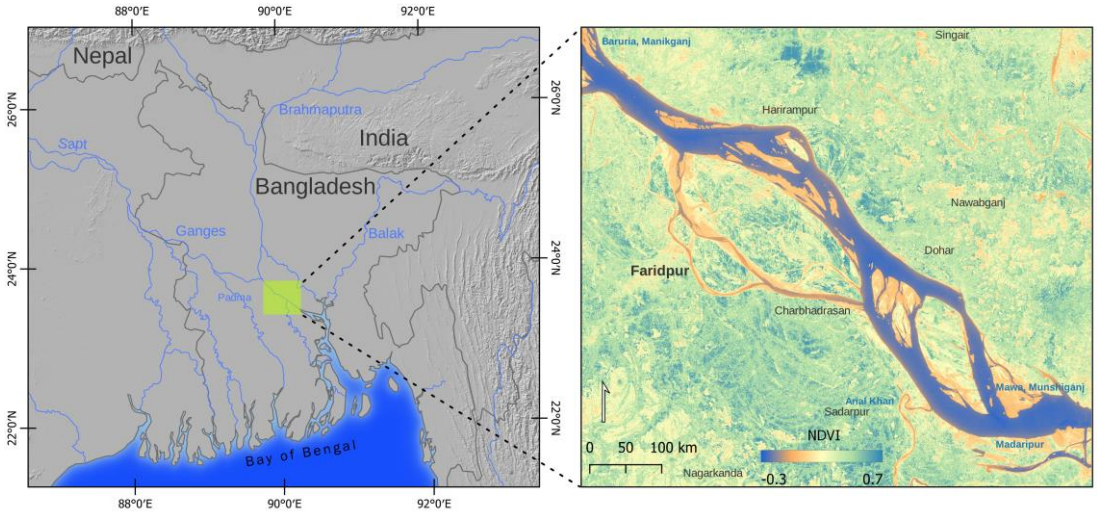

Figure 1. Study area of Padma River, Bangladesh (Source: OpenStreetMap Contributors, Natural Earth, Mapzen Global Terrain).

The study reach is about 50 km in length, demarcated as from Baruria, Manikganj to Mawa, Munsiganj, just before the Padma bridge (Figure 1). Before Mawa, an outflow called Arial Khan diverges from the main channel, but no tributaries enter the reach. The selected area is highly dynamic, with a diversified landform, ranging in width from less than 2 km to 12 km. The maximum discharge is about 75,000 m^3/s during the monsoon, and the minimum is about 5000 m^3/s during the dry/winter season [66]. Mean annual rainfall is about 2000 mm and mostly occurs during the monsoon [67]. After the monsoon, in-channel emergent sediment units appear, which are used for the cultivation of a variety of crops.

2.2. Geomorphic Classification of GUs

Geomorphic classification of GUs followed the approach of Rinaldi et al. [3]. The spatial setting for the GU analysis was bankfull channel width, which comprises (i) 'submerged' channel units (main and secondary); (ii) 'emergent' sediment units (bars, islands, inactive channels); and (iii) in-channel vegetation units. All of these are called macro-units. Macro-units are further divided into units and sub-units. GU names and classified codes were adopted from Rinaldi et al. [3], except water depression (WD) and sub-units (Table 1).

Table 1. Names and identification codes of macro-units, units, and sub-units used in the present classification.

Macro-Units		Units		Sub-Units	
Name	**Code**	**Name**	**Code**	**Name**	**Code**
Submerged channel units	C S	Main channel	C	-	-
		Secondary channel	S	-	-
Emergent sediment units	E	Bank-attached bar	EA	Side bar	SB
		Mid-channel bar	EC	Longitudinal bar	L
				Transverse bar	T
		Dry channel	ED	-	-
		Unvegetated bank	EK	-	-
		Water depression	WD	-	-
In-channel vegetation units	V	Island	VI	-	-
		Water depression	WD	-	-

2.3. Seasonal Breakdown and Image Selection

Data for 2016–2020 river discharge were collected from the Bangladesh Water Development Board (BWDB) (Figure 2). Based on these, four seasons of monsoon, post-monsoon, dry/winter, and pre-monsoon were identified. These were considered relevant temporal periods, for which satellite images could be used for the analysis. Additional criteria of image selection were (i) coverage of the study area, (ii) sensing date (considering seasons), (iii) mission type (Sentinel 2A/2B), (iv) product type (level 1C), and (v) percentage of cloud cover. Remotely sensed, multi-spectral satellite data (Sentinel 2) of consecutive years (2019–2020) were collected from the Copernicus Open Access Hub (https://scihub.copernicus.eu/dhus/#/home, accessed on 25 January 2022). Details of the satellite images are summarized in Table 2.

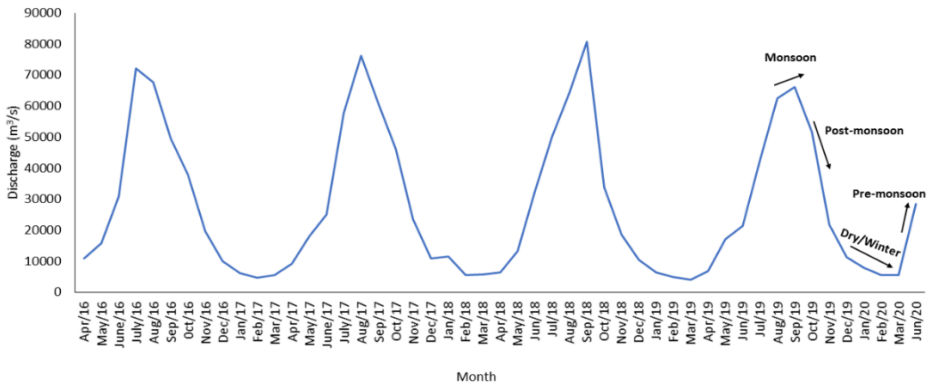

Figure 2. Monthly mean discharge data from 2016 to 2020 of the study area in Padma River, Bangladesh.

Table 2. Description of the Sentinel 2 level 1 product (S2MSI1C) used during the present study.

Satellite/Sensor	Acquisition Date	Season	Tile Identifier	Cloud Cover (%)
Sentinel 2A/MSI	19 September 2019	Monsoon 2019	45QYG	2.64
Sentinel 2A/MSI	19 September 2019	Monsoon 2019	45QZG	4.56
Sentinel 2B/MSI	11 November 2019	Post-monsoon 2019	45QYG	0
Sentinel 2B/MSI	11 November 2019	Post-monsoon 2019	45QZG	0.85
Sentinel 2B/MSI	11 February 2020	Dry/Winter 2020	45QYG	0
Sentinel 2B/MSI	11 February 2020	Dry/Winter 2020	45QZG	0
Sentinel 2B/MSI	16 April 2020	Pre-monsoon 2020	45QYG	0.12
Sentinel 2B/MSI	16 April 2020	Pre-monsoon 2020	45QZG	4.17
Sentinel 2B/MSI	11 May 2020	Pre-monsoon 2020	45QYG	47.05
Sentinel 2B/MSI	11 May 2020	Pre-monsoon 2020	45QZG	52.10

2.4. Image Processing and Analysis

The Sentinel-2 Level-1C image products provide geocoded top-of-atmosphere (TOA) reflectance after computation of cloud (opaque/cirrus) and land/water masks, based on spectral criteria [38]. Image processing and analysis were performed in QGIS, following the steps shown in Figure 3.

(a) After collection, an atmospheric correction (Dark Object Subtraction, DOS1 [68]) was applied to all the images, using the semi-automatic classification plugin (SCP) tool for QGIS [69]. Mosaics of image pairs were created to cover the study area and, consequently, subsetted to the area of interest using the bands needed to calculate NDVI (Band 4—Red and Band 8—Near-Infrared). After subsetting, the study area was devoid of cloud cover except pre-monsoon 2020. Therefore, for pre-monsoon 2020, four images were used. The first images of May 2020 were used for obtaining cloud-free areas, and after subsetting, the study area was subject to about 5% cloud cover. Using a cloud mask, two images of April 2020 were used to replace the cloud pixels (Figure 3, i–v).

(b) NDVI values range from −1 to 1. Generally, the value approaching −1 represents water; the value varying from −0.1 to 0.1 corresponds to barren areas of sand, and a value greater than 0.1 corresponds to vegetated areas [44,70]. Using visible red (Band 4) and near-infrared (Band 8) bands of Sentinel-2 data, NDVI was calculated and used to classify and analyze images. Based on the NDVI value, GUs were reclassified as land (emergent) and water (submerged). During the conversion from raster to vector, a 10% sieve analysis was performed to remove small polygons of 10 square meters in size from the result (Figure 3, vi–viii).

(c) The study area was delineated based on the image of the dry/winter season (February 2020). Next, all the GUs were classified into units and sub-units based on position and shape, i.e., location of GUs in the main channel or secondary channel and orientation of GUs towards the flow direction. After applying zonal statistics, the end product of the analysis was classified as geomorphic units with counted pixels, mean NDVI value, surface area, perimeter, and maximum distance between two vertices of each polygon (Figure 3, ix–xii).

(d) Inundated GUs or portions of GUs in high flow seasons that emerged during other seasons were termed nutrient retention- or export-relevant geomorphic units (NREGUs). Thus, classified GUs of the monsoon season (high flow) were overlapped with other seasons, to determine the nutrient retention-relevant terrestrial geomorphic units or emergent sediment units. The extraction of NREGUs was based on assumptions that (i) in large rivers, discharge is the main factor regulating nutrient retention or export [8,12,13]; (ii) changes in discharge are responsible for the alteration of water residence time; (iii) the surface area of the channel and water depth are considered determining factors for nutrient retention/export [71–75]; (iv) like the riparian zone, GUs can be flooded annually and enriched with nutrients; and (v) nutrients enter into the system through runoff and sediment supply (Figure 3, xiii–xiv).

(e) The delineation and classification of GUs were first performed for the image of the dry/winter season. Therefore, to keep the exact identification of GUs in the other images, the attributes of the GUs layer were joined by their location, resulting in corresponding GUs in other seasons. Manual cross-checking was done for each GU, other than the dry/winter seasons. Further analysis of GUs was done using zonal statistics, which provided the number of counted pixels, mean, sum, variance, maximum, and minimum value of NDVI in each GU type (emergent and submerged). The polygon shape index from SAGA [76] was used, resulting in different shape index values for each NREGU. The empirical formula of the polygon shape index is:

$$\text{Polygon Shape Index} = \text{Perimeter}/[2 \times \text{Square Root } (\Pi \times \text{Area})]$$

The surface area, perimeter, and polygon shape index of different NREGUs were compared among images of different seasons, to determine the seasonal dynamics (Figure 3, xv–xvi).

(f) Geometric errors resulting from vectorizing raster data were corrected using the fix geometrics (FG) tool.

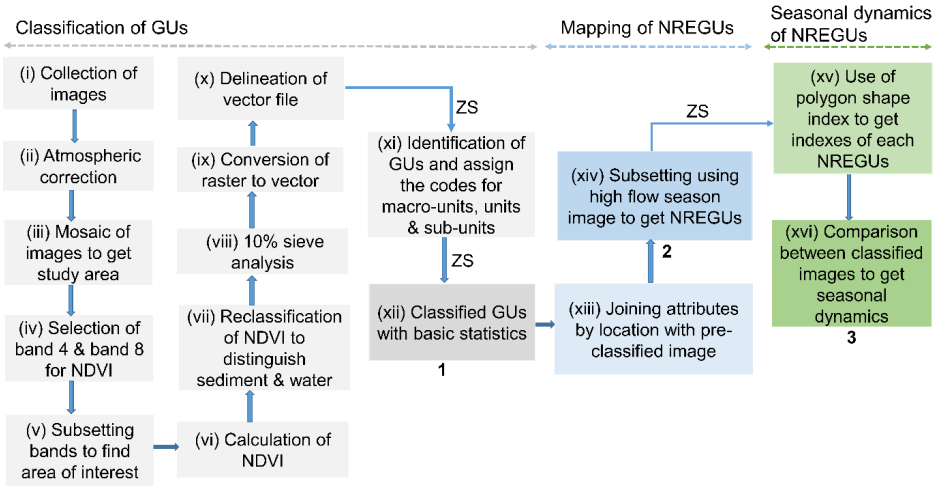

Figure 3. Work flow for the identification and categorization of geomorphic units (GUs), nutrient retention, or export relevant geomorphic units (NREGUs) and their seasonal dynamics using Sentinel-2 images. The dark color of the boxes indicates different important steps of classification. **1** = Completion of geomorphic units (GUs) classification; **2** = Completion of nutrient retention or export relevant GU (NREGUs) classification; **3** = Seasonal dynamics of NREGUs. ZS= Zonal statistics.

2.5. Field Observation and Morphometric Analysis of NREGUs

A field validation study was conducted during the dry/winter season. During the field visit, spot identification of GUs was recorded with a smartphone, using the Input app (https://inputapp.io, accessed on 25 January 2022). This app is linked with a repository of geodata (Mergin cloud service, https://public.cloudmergin.com, accessed on 25 January 2022) and can be synchronized within QGIS, avoiding further manual processing. NREGUs of the study reach of the previous year were developed prior to the field survey. The mean NDVI value of each NREGU was used to observe a seasonal variation. Besides NDVI, polygon shape index, surface area, perimeter area ratio (P/A), and maximum distance of NREGUs were used for the morphometric analysis of NREGUs. Regression analysis was performed, to determine the primary determinant of polygon shape index, which can show the suitability of the shape index to differentiate the sub-units longitudinal (L) and transverse bar (T). The analysis was performed in R v4.1.2 [77].

3. Results

3.1. Identification of GUs and Seasonal Dynamics

The geomorphic mapping showed that the study area consisted of three macro-units and seven sub-units. The macro-units are baseflow or submerged units (C/S), emergent sediment units (E), and in-channel vegetation (V). The units were categorized as primary and secondary channels (C & S), mid-channel bar (EC), bank-attached bar (EA), unvegetated bank (EK), dry channel (ED), island (VI), and water depression (WD). Further EC were classified into the sub-units, longitudinal bar (L) and transverse bar (T), and EA into the side bar (SB).

The identified types of GUs were observed in all four seasons, except ED in the monsoon. The surface area of C/S was maximum during monsoon and minimum during the dry/winter season (Figure 4). However, the numbers of E and V were highest during pre-monsoon. An inverse relationship between discharge (m^3/s) and surface area of E and

V was observed throughout the study year. The number of GUs varied with discharge. When water level increased, inundation split the bars (E) and islands (V), increasing the number, but reducing the surface area. This phenomenon was primarily observed pre-monsoon. During the dry/winter season, the surface area of E and V increased, with concomitant reductions in their number (Figure 5).

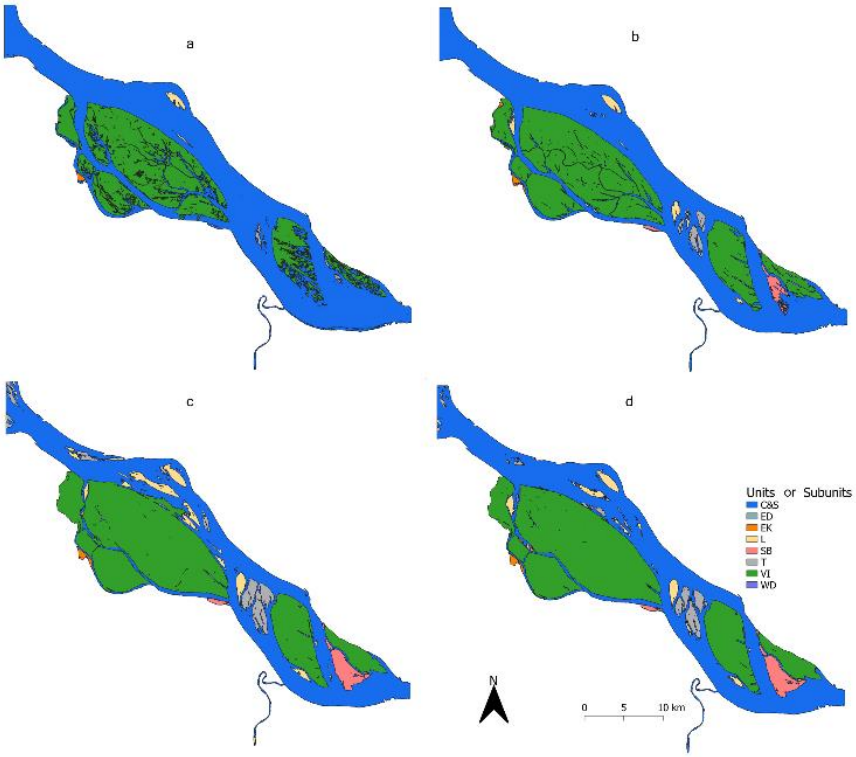

Figure 4. Geomorphic units (GUs) of the Padma River, Bangladesh during (**a**) monsoon 2019, (**b**) post-monsoon 2019, (**c**) dry/winter 2020, and (**d**) pre-monsoon 2020.

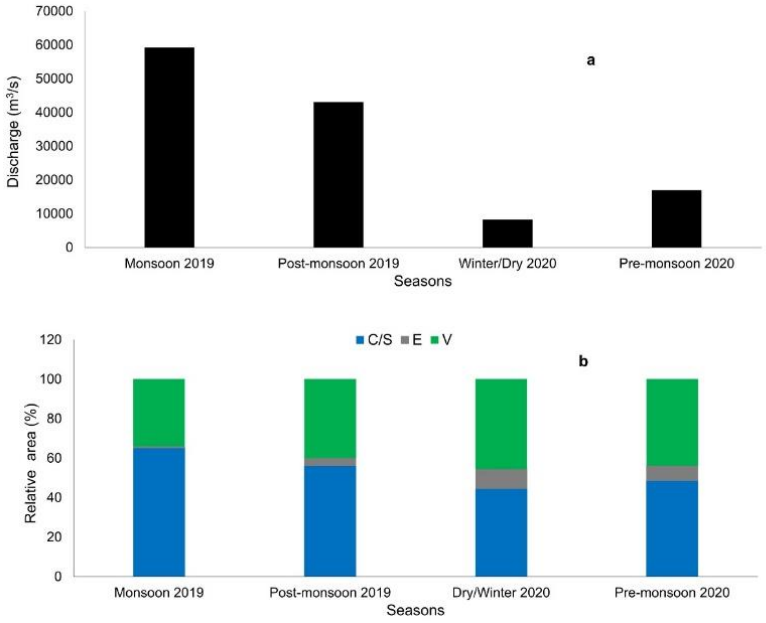

Figure 5. Seasonal changes of (**a**) discharge and (**b**) surface area of GUs (macro-unit level) of the Padma River, Bangladesh during monsoon 2019, post-monsoon 2019, dry/winter 2020, and pre-monsoon 2020.

3.2. Seasonal Variation of NREGUs

Mapping of estimated nutrient retention or export-related GUs (NREGUs) showed that the remaining bars accounted for only 0.96% of surface area during the monsoon, and all of this was in EC. The maximum surface area of C & S was observed during the monsoon season (92.6%), followed by the post-monsoon season (87.5%), and the minimum was observed during the dry/winter season (63.5%). Among the emergent units, the surface area of VI was the maximum, followed by EC, EA, EK, and ED. The maximum surface areas of VI and EC were observed during the dry/winter season (VI = 21.9% and EC = 10.49%), and the minimum during the monsoon season (VI = 3.79% and EC = 0.96%). The surface areas of ED and EK were higher in the post-monsoon season than in the dry/winter season (Figure 6 and Table 3). Such a result was found because, in the dry/winter season, some of the ED and EK portions merged as islands. As with GUs, the seasonal prevalence of NREGUs was related to discharge.

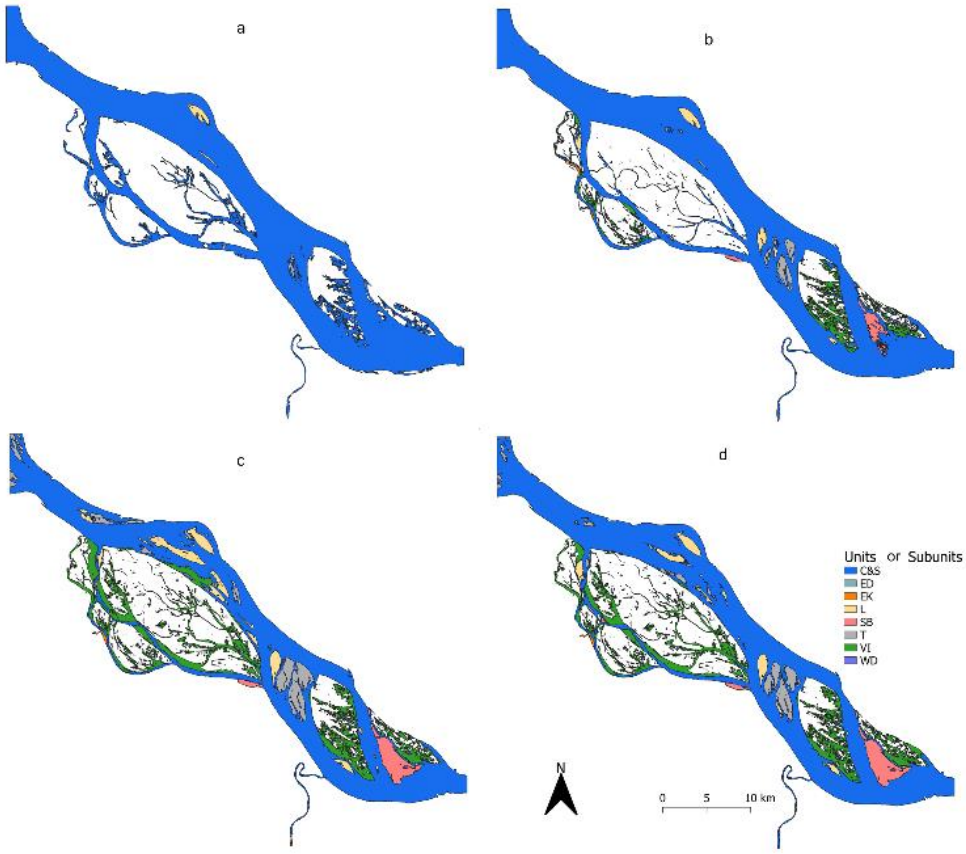

Figure 6. Nutrient retention or export-related GUs of the Padma River, Bangladesh during (**a**) monsoon 2019, (**b**) post-monsoon 2019, (**c**) dry/winter 2020, and (**d**) pre-monsoon 2020.

Table 3. The surface area of NREGUs in the Padma River, Bangladesh in km^2 and percentage.

GU	Monsoon		Post-Monsoon		Dry/Winter		Pre-Monsoon	
	km^2	%	km^2	%	km^2	%	km^2	%
C&S	362.58	92.6	315.0	87.53	250.88	63.52	274.75	77.0
EA	0.00	-	0.69	0.19	13.29	3.36	13.49	3.78
EC	3.78	0.96	13.25	3.68	41.43	10.49	24.1	6.76
ED	0.00	-	0.30	0.08	0.1	0.02	0.03	0.01
EK	0.00	-	0.94	0.26	0.57	0.14	0.53	0.15
VI	14.83	3.79	26.2	7.28	86.5	21.90	42.9	12.0
WD	10.34	2.64	3.48	0.97	2.2	0.56	0.98	0.28

3.3. Use of NDVI and Shape Indexes for Morphometric Analysis

The identification of GUs and NREGUs was mainly based on NDVI. The mean NDVI value of each NREGU showed that it explicitly differentiated channels (C & S), bars (SB, T and L), and islands (VI), and that these NREGUs represent a high proportion of the study area. The NDVI value of C & S was always less than 0, but varied across seasons. This finding demonstrated the effectiveness of the use of NDVI in the seasonal classification of NREGUs. NDVI values showed the expected results in the case of bars (0.1 < median NDVI < 0.2) and islands (median NDVI > 0.2). The bars were primarily sandy units with or without vegetation, whereas islands are the main vegetated units, showing higher NDVI than bars. The NDVI value of WD was around 0, because these were the shallow water portions inside islands or bars, represented by a relatively small surface area. The identification of NREGUs was validated by field observations during the dry/winter

season. NDVI values from the field identified C & S, bars, and VI corresponding to the derived values of satellite identified NREGUs (Figure 7).

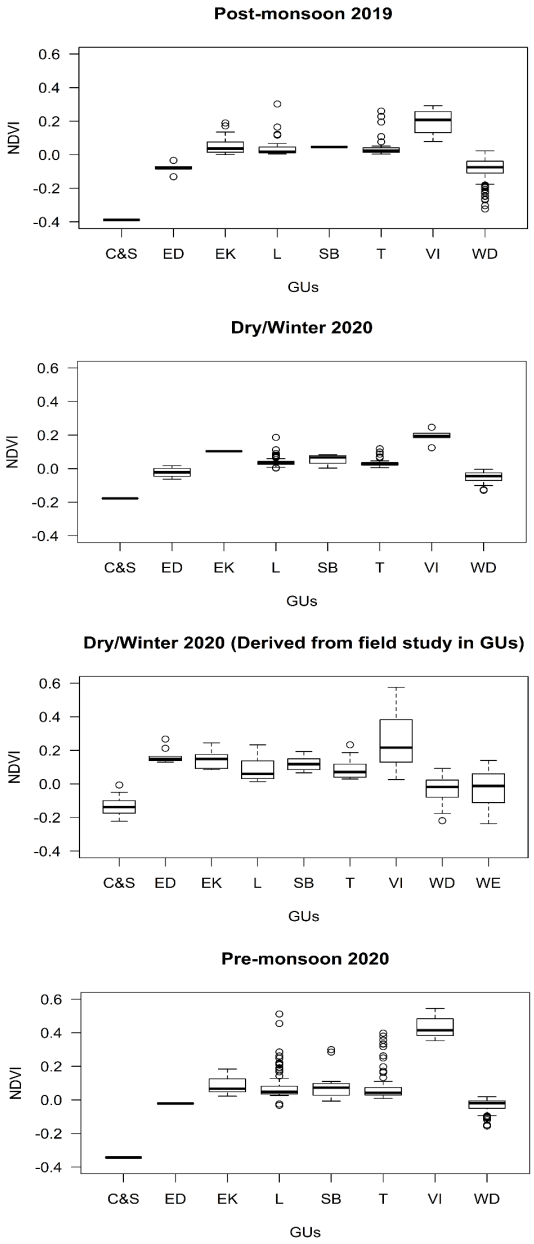

Figure 7. Mean NDVI value of NREGUs during different seasons in the Padma River, Bangladesh.

Shape characterization shows the variation of spatial data. During the present study, the NDVI value was not useful to differentiate among the bar subtypes, but the polygon shape index and perimeter/area were useful. The polygon shape index distinguished longitudinal bar (L) and transverse bar (T) during post-monsoon and dry/winter, where the median value of L was greater than 2 and T was less than 2. However, during pre-monsoon, the polygon shape index did not show satisfactory results when the median value of the polygon shape index was near 2. This happened due to the divergent nature of the bars; i.e., splitting of the bars occurred due to an increase of water volume. The perimeter area ratio (P/A) differentiated L and T during pre-monsoon, when the median values of L and T were above and below 0.1, respectively (Figure 8).

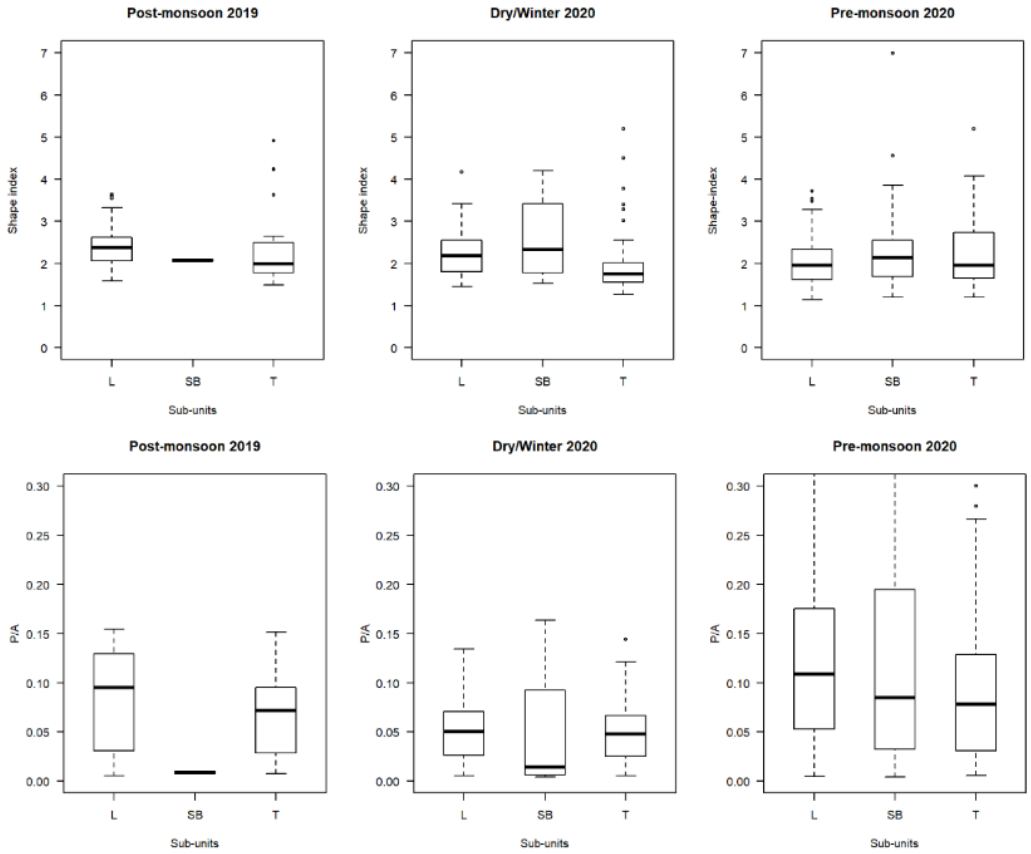

Figure 8. Polygon shape index (shape index) and perimeter and area ratio (P/A) of longitudinal (L), transverse (T), and side bar (SB) in post-monsoon 2019, dry/winter 2020, and pre-monsoon 2020 in Padma River, Bangladesh.

The regression analysis between polygon shape index and different parameters (area, perimeter, and maximum distance) of the longitudinal bar (L) and transverse bar (T) in three seasons showed that the R^2 value was higher in the case of perimeter, followed by maximum distance and area (Figure 9). As such, the perimeter was the important parameter that most impacted the value of the polygon shape index. This finding mainly validated the categorization of bars. The finding even supported the results during post-monsoon and dry/winter seasons, when the shape index differentiated L and T. Thus, polygon shape index was essential for classifying the subtypes of the bar. Comparatively lower R^2 values (L = 0.541; T = 0.4742) during pre-monsoon for perimeter compared with shape index were evidence that the polygon shape index did not help differentiate between L and T, but perimeter area ratio (P/A) was effective in that case (Figures 8 and 9).

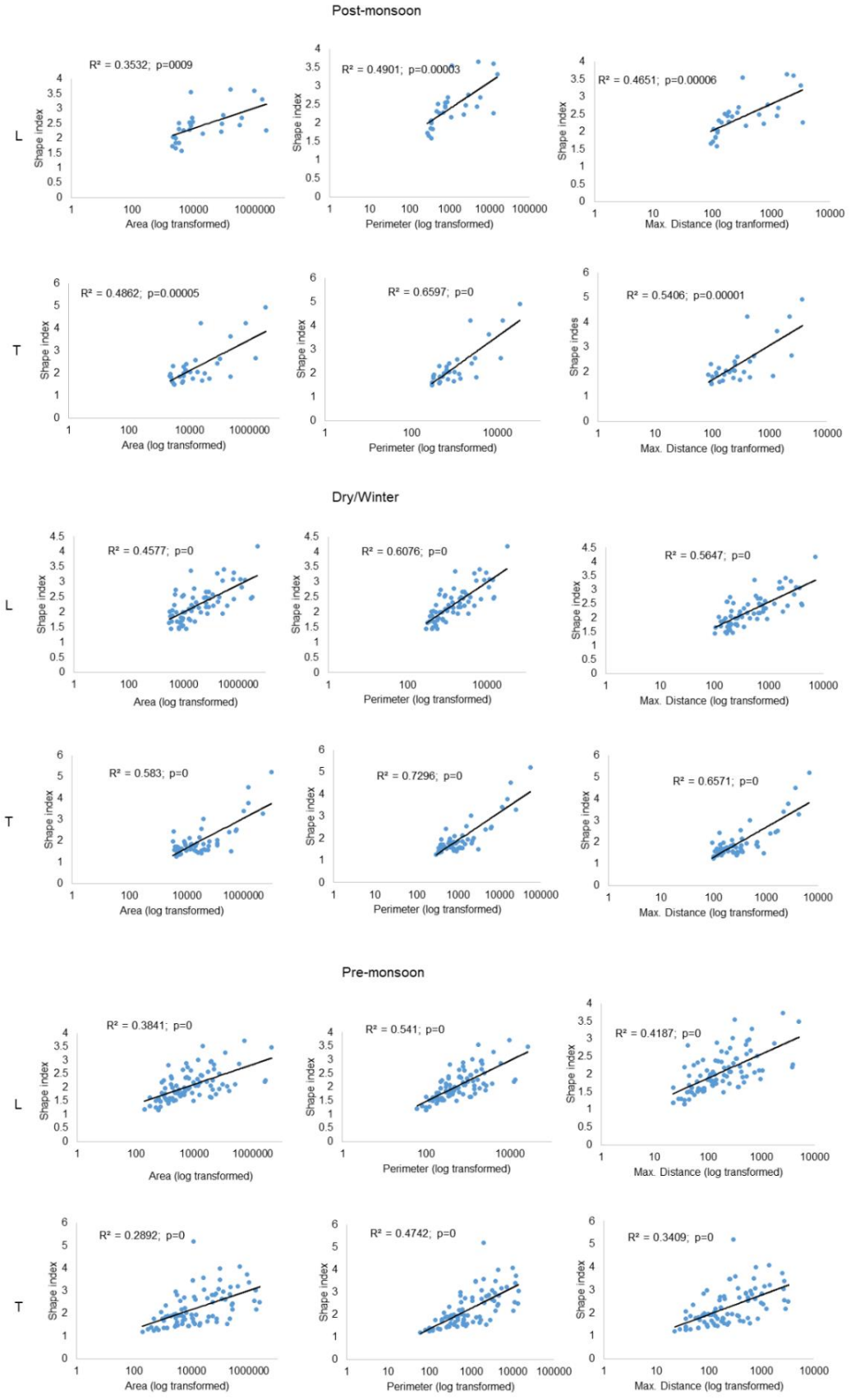

Figure 9. Linear regression between shape index and surface area, perimeter, and maximum distance of longitudinal bar (L) and transverse bar (T) during post-monsoon-2019, dry/winter 2020, and pre-monsoon 2020 Padma River, Bangladesh.

4. Discussion

River hydromorphology plays a role in ecological processes, habitat structure, and water quality [78,79]. Classification of GUs in rivers aids the assessment of seasonal or long-term hydromorphological alterations [6]. Previously, GUs of the upper part of the Padma River were identified and categorized as active channel, mid channel bar, lateral bar deposit, new bar deposit, old bar deposit, abandoned channel deposit, and flood plain deposit, to assess its morphological pattern over the decade using sinuosity ratio, braided index, and percentage of islands [80]. The present classification scheme incorporates an NDVI-based seasonal approach, which can be used to establish links between hydromorphology and biogeochemical processes of the river reach.

It has been observed that erosion and deposition at GUs in large lowland rivers are related to the seasonal discharges [81] that drive hydrological and sediment dynamics [67,82]. The present study illustrates the importance of seasonal discharge for the surface area and number of GUs, and how this affects NREGUs and, hence, nutrient flux in large rivers [13,83]. In the Padma River, the area of bars (E) and islands (VI) have increased over the years [67,84,85]. This has implications for the nutrient dynamics in the river, changing flow velocity, and water residence time. The maximum exposed surface area of E and VI of the study reach was observed during the dry/winter season. Low water flows were prevalent during the winter/dry season, associated with a comparatively large portion of emergent sediment units. Nawfee et al. [84] observed the characteristics of the river over a period from 1973 to 2014, where the erosion–deposition process of the bars was stable during the low flooding season (dry/winter season) and can be described as a geomorphologically dynamic equilibrium state [86–88]. Some of the geomorphically complex large rivers consist of a significant portion of vegetated islands, due to the stable state [80,89–91]. Some portions of bars are used for cultivation and can present various LULC patterns in different seasons.

The finer resolution of Sentinel-2 was found to be useful, as it identified WD in different seasons. This also showed the applicability of NDVI over NDWI. The WD might be potentially important for nutrient retention, due to its capacity for retaining water for a longer period than other GUs, making the environment favorable for biogeochemical processes. Several studies have shown high denitrification rates in wetlands, related to temporal water retention [92–94]. Unlike other studies [95–97], the mean NDVI values of the VI in NREGUs in our study were below 0.6 in all seasons, because the study area consisted of only low growing vegetation, without trees or shrubs. Therefore, over saturation of NDVI due to dense vegetation might not be considered a hindrance for the present research and provides the effectiveness of NDVI over EVI. However, the latter is considered more suitable than NDVI in some remote sensing studies [98–100].

NDVI can be used to classify land cover to some degree [101] and estimate nutrient retention [102,103]. Classification of NREGUs based on NDVI provides the potential to categorize vegetation nutrient retention. Studies on the Parana River in Argentina showed that vegetation is closely linked with geomorphic units [59]. Recently NDVI has been implemented for crop classification and irrigation water monitoring [43,52,104]; both might be favorable for the present study, due to inundation and human-induced LULC types. In the GUs of the Padma River, both natural and human-induced vegetation were observed. Especially in the islands (VI) and bars (E), the vegetation cover and types were different. There is strong evidence that biogeochemical processes such as plant uptake and denitrification can vary according to vegetation cover and type [105–107]. Thus, NDVI-based LULC mapping might be useful to predict the spatial and temporal variation of nutrient retention processes of the study reach and other similar river systems.

Shape characterization is important for mapping and delineating in-channel GUs and describing spatiotemporal changes of GUs [5,108]. The position and geometry of the bars change over time in the Padma River [80]. A significant association was observed during the present study between polygon shape index and perimeter from post-monsoon to dry/winter seasons, when water depth and discharge decreased. This finding could be

associated with other seasonal measurements of nutrient retention processes, to determine the impact of the shape of the bars. Alternatively, the spatial variation of nutrient retention of a geomorphically complex river can be linked, by determining the geometry of the bars, i.e., shape characterization, because discharge plays a vital role in both cases.

5. Conclusions

The NDVI based GU classification scheme provides a new approach for assessing GUs in large geomorphically complex lowland rivers. The use of NDVI brings the opportunity to incorporate vegetation and LULC. Thus, LULC types in GUs can be considered patches that might be useful to link with the biogeochemical and ecological processes of river systems. Mean NDVI distinguished, not only primary and secondary channels (C & S), islands (VI), and bars (EC), but also changes across seasons. This finding indicates the effectiveness of NDVI-based classification. The study confirmed that seasonal discharge could significantly change the surface area of water and sediment portions of the river channel. The present study also showed that morphometric parameters, i.e., polygon shape index, help categorize the types of bar, such as longitudinal (L) and transverse (T), where NDVI was ineffective. The perimeter of the bars (L and T) is the primary determiner of the polygon shape index. This provides the potential for using shape index to estimate the spatiotemporal variation of nutrient retention processes among in-channel emergent sediment units, which can be further tested with field research. The approach we presented here should also be tested with complementary direct and indirect techniques using other satellite data.

Author Contributions: Conceptualization, M.A.G., M.E.M. and K.I.; methodology, M.A.G. and J.v.d.K.; software, M.A.G. and J.v.d.K.; validation, M.A.G., J.v.d.K. and G.G.; formal analysis, M.A.G.; investigation, M.A.G., J.v.d.K. and G.G.; resources M.A.G. and J.v.d.K.; data curation, M.A.G., J.v.d.K. and G.G.; writing—original draft preparation, M.A.G. and J.v.d.K.; writing—review and editing, M.A.G., J.v.d.K., M.E.M., G.G. and K.I.; visualization, M.A.G. and J.v.d.K.; supervision, M.E.M. and K.I.; project administration, M.E.M. and K.I.; funding acquisition, M.A.G. All authors have read and agreed to the published version of the manuscript.

Funding: The financial support was provided by the Bangabandhu Science and Technology Fellowship Trust, Ministry of Science and Technology, The Government People's Republic of Bangladesh. The APC was funded by IHE Delft Institute for Water Education, Delft, The Netherlands.

Institutional Review Board Statement: Not applicable.

Informed Consent Statement: Not applicable.

Data Availability Statement: Requests for materials used in the present research should be addressed to M.A.G.

Conflicts of Interest: The authors declare no conflict of interest.

References

1. Fryirs, K.A.; Brierley, G.J. *Geomorphic Analysis of River Systems: An Approach to Reading the Landscape*; John Wiley & Sons, Ltd.: Hoboken, NJ, USA, 2013; ISBN 9781741382983.
2. Elosegi, A.; Pozo, J. Altered Organic Matter Dynamics in Rivers and Streams: Ecological Consequences and Management Implications. *Limnetica* **2016**, *35*, 303–322. [CrossRef]
3. Rinaldi, M.; Belletti, B.; Comiti, F.; Nardi, L.; Bussettini, M.; Mao, L.; Gurnel, A.M. *The Geomorphic Units Survey and Classification System (GUS), Deliverable 6.2, Part 4, of REFORM (REstoring Rivers FOR Effective Catchment Management), a Collaborative Project (Large-Scale Integrating Project) Funded by the European Commission within the 7th Framework Programme under Grant Agreement 282656*; 2015. Available online: https://www.researchgate.net/publication/283539400_The_Geomorphic_Units_survey_and_classification_System_GUS_Deliverable_62_Part_4_of_REFORM_REstoring_rivers_FOR_effective_catchment_Management_a_Collaborative_project_large-scale_integrating_project_fu (accessed on 25 January 2022).
4. Wyrick, J.R.; Pasternack, G.B. Geospatial Organization of Fluvial Landforms in a Gravel-Cobble River: Beyond the Riffle-Pool Couplet. *Geomorphology* **2014**, *213*, 48–65. [CrossRef]
5. Wheaton, J.M.; Fryirs, K.A.; Brierley, G.; Bangen, S.G.; Bouwes, N.; O'Brien, G. Geomorphic Mapping and Taxonomy of Fluvial Landforms. *Geomorphology* **2015**, *248*, 273–295. [CrossRef]

6. Belletti, B.; Rinaldi, M.; Bussettini, M.; Comiti, F.; Gurnell, A.M.; Mao, L.; Nardi, L.; Vezza, P. Geomorphology Characterising Physical Habitats and Fl Uvial Hydromorphology: A New System for the Survey and Classi Fi Cation of River Geomorphic Units. *Geomorphology* **2017**, *283*, 143–157. [CrossRef]
7. Sigleo, A.C.; Frick, W.E. Seasonal Variations in River Discharge and Nutrient Export to a Northeastern Pacific Estuary. *Estuar. Coast. Shelf Sci.* **2007**, *73*, 368–378. [CrossRef]
8. De Klein, J.J.M.; Koelmans, A.A. Quantifying Seasonal Export and Retention of Nutrients in West European Lowland Rivers at Catchment Scale. *Hydrol. Processes* **2011**, *25*, 2102–2111. [CrossRef]
9. Jossette, G.; Leporcq, B.; Sanchez, N. Philippon Biogeochemical Mass-Balances (C, N, P, Si) in Three Large Reservoirs of the Seine Basin (France). *Biogeochemistry* **1999**, *47*, 119–146. [CrossRef]
10. Bernot, M.J.; Dodds, W.K. Nitrogen Retention, Removal, and Saturation in Lotic Ecosystems. *Ecosystems* **2005**, *8*, 442–453. [CrossRef]
11. Grizzetti, B.; Passy, P.; Billen, G.; Bouraoui, F.; Garnier, J.; Lassaletta, L. The Role of Water Nitrogen Retention in Integrated Nutrient Management: Assessment in a Large Basin Using Different Modelling Approaches. *Environ. Res. Lett.* **2015**, *10*, 065008. [CrossRef]
12. Krishna, M.S.; Prasad, M.H.K.; Rao, D.B.; Viswanadham, R.; Sarma, V.V.S.S.; Reddy, N.P.C. ScienceDirect Export of Dissolved Inorganic Nutrients to the Northern Indian Ocean from the Indian Monsoonal Rivers during Discharge Period. *Geochim. Cosmochim. Acta* **2016**, *172*, 430–443. [CrossRef]
13. Best, J. Anthropogenic Stresses on the World's Big Rivers. *Nat. Geosci.* **2019**, *12*, 7–21. [CrossRef]
14. Eisner, S.; Flörke, M.; Chamorro, A.; Daggupati, P. An Ensemble Analysis of Climate Change Impacts on Streamflow Seasonality across 11 Large River Basins. *Clim. Change* **2017**, *141*, 401–417. [CrossRef]
15. Soar, P.J.; Wallerstein, N.P.; Thorne, C.R. Quantifying River Channel Stability at the Basin Scale. *Water* **2017**, *9*, 133. [CrossRef]
16. Cheng, F.Y.; Basu, N.B. Biogeochemical Hotspots: Role of Small Water Bodies in Landscape Nutrient Processing. *Water Resour. Res.* **2017**, *53*, 5038–5056. [CrossRef]
17. Balestrini, R.; Arese, C.; Delconte, C.A.; Lotti, A.; Salerno, F. Nitrogen Removal in Subsurface Water by Narrow Buffer Strips in the Intensive Farming Landscape of the Po River Watershed, Italy. *Ecol. Eng.* **2011**, *37*, 148–157. [CrossRef]
18. Balestrini, R.; Arese, C.; Delconte, C. Nitrogen Removal in a Freshwater Riparian Wetland: An Example from an Italian Lowland Spring. *Internationale Vereinigung für Theoretische und Angewandte Limnologie Verhandlungen* **2006**, *29*, 2217–2220. [CrossRef]
19. Walton, C.R.; Zak, D.; Audet, J.; Petersen, R.J.; Lange, J.; Oehmke, C.; Wichtmann, W.; Kreyling, J.; Grygoruk, M.; Jabłońska, E.; et al. Wetland Buffer Zones for Nitrogen and Phosphorus Retention: Impacts of Soil Type, Hydrology and Vegetation. *Sci. Total Environ.* **2020**, *727*, 138709. [CrossRef]
20. Masoud, A.A. On the Retrieval of the Water Quality Parameters from Sentinel-3/2 and Landsat-8 OLI in the Nile Delta's Coastal and Inland Waters. *Water* **2022**, *14*, 593. [CrossRef]
21. Li, S.; Chen, F.; Song, K.; Liu, G.; Tao, H.; Xu, S.; Wang, X.; Wang, Q.; Mu, G. Mapping the Trophic State Index of Eastern Lakes in China Using an Empirical Model and Sentinel-2 Imagery Data. *J. Hydrol.* **2022**, *608*, 127613. [CrossRef]
22. De Stefano, L.G.; Valdivia, A.S.; Gianello, D.; Gerea, M.; Reissig, M.; García, P.E.; García, R.D.; Cárdenas, C.S.; Diéguez, M.C.; Queimaliños, C.P.; et al. Using CDOM Spectral Shape Information to Improve the Estimation of DOC Concentration in Inland Waters: A Case Study of Andean Patagonian Lakes. *Sci. Total Environ.* **2022**, *824*, 153752. [CrossRef]
23. Zeng, S.; Du, C.; Li, Y.; Lyu, H.; Dong, X.; Lei, S.; Li, J.; Wang, H. Monitoring the Particulate Phosphorus Concentration of Inland Waters on the Yangtze Plain and Understanding Its Relationship with Driving Factors Based on OLCI Data. *Sci. Total Environ.* **2022**, *809*, 151992. [CrossRef] [PubMed]
24. Kratzer, S.; Kyryliuk, D.; Edman, M.; Philipson, P.; Lyon, S. Synergy of Satellite, In Situ and Modelled Data for Addressing the Scarcity of Water Quality Information for Eutrophication Assessment and Monitoring of Swedish Coastal Waters. *Remote Sens.* **2019**, *11*, 2051. [CrossRef]
25. Wang, S.; Li, J.; Zhang, B.; Spyrakos, E.; Tyler, A.N.; Shen, Q.; Zhang, F.; Kuster, T.; Lehmann, M.K.; Wu, Y.; et al. Trophic State Assessment of Global Inland Waters Using a MODIS-Derived Forel-Ule Index. *Remote Sens. Environ.* **2018**, *217*, 444–460. [CrossRef]
26. Fay, A.R.; McKinley, G.A. Correlations of Surface Ocean PCO2 to Satellite Chlorophyll on Monthly to Interannual Timescales. *Glob. Biogeochem. Cycles* **2017**, *31*, 436–455. [CrossRef]
27. Binding, C.E.; Greenberg, T.A.; Watson, S.B.; Rastin, S.; Gould, J. Long Term Water Clarity Changes in North America's Great Lakes from Multi-Sensor Satellite Observations. *Limnol. Oceanogr.* **2015**, *60*, 1976–1995. [CrossRef]
28. De Grandpré, A.; Kinnard, C.; Bertolo, A. Open-Source Analysis of Submerged Aquatic Vegetation Cover in Complex Waters Using High-Resolution Satellite Remote Sensing: An Adaptable Framework. *Remote Sens.* **2022**, *14*, 267. [CrossRef]
29. Wieland, M.; Martinis, S. A Modular Processing Chain for Automated Flood Monitoring from Multi-Spectral Satellite Data. *Remote Sens.* **2019**, *11*, 2330. [CrossRef]
30. Kwak, Y. Nationwide Flood Monitoring for Disaster Risk Reduction Using Multiple Satellite Data. *ISPRS Int. J. Geo-Inf.* **2017**, *6*, 203. [CrossRef]
31. Ahamed, A.; Bolten, J.D. A MODIS-Based Automated Flood Monitoring System for Southeast Asia. *Int. J. Appl. Earth Obs. Geoinf.* **2017**, *61*, 104–117. [CrossRef]

32. Guilhen, J.; al Bitar, A.; Sauvage, S.; Parrens, M.; Martinez, J.-M.; Abril, G.; Moreira-Turcq, P.; Sánchez-Pérez, J.-M. Denitrification and Associated Nitrous Oxide and Carbon Dioxide Emissions from the Amazonian Wetlands. *Biogeosciences* **2020**, *17*, 4297–4311. [CrossRef]
33. Martínez-Espinosa, C.; Sauvage, S.; al Bitar, A.; Green, P.A.; Vörösmarty, C.J.; Sánchez-Pérez, J.M. Denitrification in Wetlands: A Review towards a Quantification at Global Scale. *Sci. Total Environ.* **2021**, *754*, 142398. [CrossRef] [PubMed]
34. Faruque, M.J.; Vekerdy, Z.; Hasan, M.Y.; Islam, K.Z.; Young, B.; Ahmed, M.T.; Monir, M.U.; Shovon, S.M.; Kakon, J.F.; Kundu, P. Monitoring of Land Use and Land Cover Changes by Using Remote Sensing and GIS Techniques at Human-Induced Mangrove Forests Areas in Bangladesh. *Remote Sens. Appl. Soc. Environ.* **2022**, *25*, 100699. [CrossRef]
35. Gameiro, S.; Nascimento, V.; Facco, D.; Sfredo, G.; Ometto, J. Multitemporal Spatial Analysis of Land Use and Land Cover Changes in the Lower Jaguaribe Hydrographic Sub-Basin, Ceará, Northeast Brazil. *Land* **2022**, *11*, 103. [CrossRef]
36. Ge, G.; Zhang, J.; Chen, X.; Liu, X.; Hao, Y.; Yang, X.; Kwon, S.M. Effects of Land Use and Land Cover Change on Ecosystem Services in an Arid Desert-Oasis Ecotone along the Yellow River of China. *Ecol. Eng.* **2022**, *176*, 106512. [CrossRef]
37. Markogianni, V.; Kalivas, D.; Petropoulos, G.P.; Dimitriou, E. Modelling of Greek Lakes Water Quality Using Earth Observation in the Framework of the Water Framework Directive (WFD). *Remote Sens.* **2022**, *14*, 739. [CrossRef]
38. SUHET. *Sentinel-2 User Handbook*; European Space Agency: Paris, France, 2015; pp. 1–64.
39. Drusch, M.; del Bello, U.; Carlier, S.; Colin, O.; Fernandez, V.; Gascon, F.; Hoersch, B.; Isola, C.; Laberinti, P.; Martimort, P.; et al. Sentinel-2: ESA's Optical High-Resolution Mission for GMES Operational Services. *Remote Sens. Environ.* **2012**, *120*, 25–36. [CrossRef]
40. McFeeters, S.K. The Use of the Normalized Difference Water Index (NDWI) in the Delineation of Open Water Features. *Int. J. Remote Sens.* **1996**, *17*, 1425–1432. [CrossRef]
41. Serrano, J.; Shahidian, S.; Marques da Silva, J. Evaluation of Normalized Difference Water Index as a Tool for Monitoring Pasture Seasonal and Inter-Annual Variability in a Mediterranean Agro-Silvo-Pastoral System. *Water* **2019**, *11*, 62. [CrossRef]
42. Didan, K.; Barreto Munoz, A.; Solano, R.; Huete, A. *MODIS Vegetation Index User's Guide (MOD13 Series)*; University of Arizona: Tucson, AZ, USA, 2015.
43. Freden, S.C.; Mercanti, E.P.; Becker, M.A. (Eds.) *Third Earth Resources Technology Satellite-1 Symposium—Volume 1: Technical Presentations*; NASA: Washington, DC, USA, 1974; pp. 309–317.
44. Japan Association on Remote Sensing. *Remote Sensing Note*; Nihon Printing Co., Ltd.: Tokyo, Japan, 1993.
45. Sonam; Jain, V.; Fryirs, K.; Brierley, G. Geomorphic Characterization of a Seasonal River Network in Semi-Arid Western India Using the River Styles Framework. *J. Asian Earth Sci. X* **2022**, *7*, 100077. [CrossRef]
46. Fryirs, K.; Brierley, G. Assemblages of Geomorphic Units: A Building Block Approach to Analysis and Interpretation of River Character, Behaviour, Condition and Recovery. *Earth Surf. Processes Landf.* **2022**, *47*, 92–108. [CrossRef]
47. Han, M.; Brierley, G. Channel Geomorphology and Riparian Vegetation Interactions along Four Anabranching Reaches of the Upper Yellow River. *Prog. Phys. Geogr. Earth Environ.* **2020**, *44*, 898–922. [CrossRef]
48. Boz, B.; Gumiero, B. Nitrogen Removal in an Afforested Riparian Zone: The Contribution of Denitrification Processes. *Hydrobiologia* **2016**, *774*, 167–182. [CrossRef]
49. Gomez-Velez, J.D.; Harvey, J.W.; Cardenas, M.B.; Kiel, B. Denitrification in the Mississippi River Network Controlled by Flow through River Bedforms. *Nat. Geosci.* **2015**, *8*, 941–945. [CrossRef]
50. Tatariw, C.; Chapman, E.L.; Sponseller, R.A.; Mortazavi, B.; Edmonds, J.W. Denitrification in a Large River: Consideration of Geomorphic Controls on Microbial Activity and Community Structure. *Ecology* **2013**, *94*, 2249–2262. [CrossRef] [PubMed]
51. Taramelli, A.; Lissoni, M.; Piedelobo, L.; Schiavon, E.; Valentini, E.; Xuan, A.N.; González-Aguilera, D. Monitoring Green Infrastructure for Natural Water Retention Using Copernicus Global Land Products. *Remote Sens.* **2019**, *11*, 1583. [CrossRef]
52. Piedelobo, L.; Taramelli, A.; Schiavon, E.; Valentini, E.; Molina, J.-L.; Nguyen Xuan, A.; González-Aguilera, D. Assessment of Green Infrastructure in Riparian Zones Using Copernicus Programme. *Remote Sens.* **2019**, *11*, 2967. [CrossRef]
53. Piedelobo, L.; Hernández-López, D.; Ballesteros, R.; Chakhar, A.; del Pozo, S.; González-Aguilera, D.; Moreno, M.A. Scalable Pixel-Based Crop Classification Combining Sentinel-2 and Landsat-8 Data Time Series: Case Study of the Duero River Basin. *Agric. Syst.* **2019**, *171*, 36–50. [CrossRef]
54. Martín-Ortega, P.; García-Montero, L.G.; Sibelet, N. Temporal Patterns in Illumination Conditions and Its Effect on Vegetation Indices Using Landsat on Google Earth Engine. *Remote Sens.* **2020**, *12*, 211. [CrossRef]
55. Kumari, N.; Srivastava, A.; Dumka, U.C. A Long-Term Spatiotemporal Analysis of Vegetation Greenness over the Himalayan Region Using Google Earth Engine. *Climate* **2021**, *9*, 109. [CrossRef]
56. Xue, J.; Su, B. Significant Remote Sensing Vegetation Indices: A Review of Developments and Applications. *J. Sens.* **2017**, *2017*, 1353691. [CrossRef]
57. Marchetti, Z.Y.; Ramonell, C.G.; Brumnich, F.; Alberdi, R.; Kandus, P. Vegetation and Hydrogeomorphic Features of a Large Lowland River: NDVI Patterns Summarizing Fluvial Dynamics and Supporting Interpretations of Ecological Patterns. *Earth Surf. Processes Landf.* **2020**, *45*, 694–706. [CrossRef]
58. Marchetti, Z.Y.; Minotti, P.G.; Ramonell, C.G.; Schivo, F.; Kandus, P. NDVI Patterns as Indicator of Morphodynamic Activity in the Middle Paraná River Floodplain. *Geomorphology* **2016**, *253*, 146–158. [CrossRef]
59. Marchetti, Z.Y.; Latrubesse, E.M.; Pereira, M.S.; Ramonell, C.G. Vegetation and Its Relationship with Geomorphologic Units in the Parana River floodplain, Argentina. *J. South Am. Earth Sci.* **2013**, *46*, 122–136. [CrossRef]

60. Luan, J.; Liu, D.; Zhang, L.; Huang, Q.; Feng, J.; Lin, M.; Li, G. Analysis of the Spatial-Temporal Change of the Vegetation Index in the Upper Reach of Han River Basin in 2000–2016. *Proc. Proc. Int. Assoc. Hydrol. Sci.* **2018**, *379*, 287–292. [CrossRef]
61. Kaplan, G.; Avdan, U. Mapping and Monitoring Wetlands Using Sentinel-2 Satellite Imagery. ISPRS Annals of the Photogrammetry, Remote Sensing and Spatial Information Sciences. In Proceedings of the 2017 4th International GeoAdvances Workshop, Safranbolu, Turkey, 14–15 October 2017; Volume IV-4/W4, pp. 271–277.
62. Xu, W.; Yang, D.; Li, Y.; Xiao, R. Correlation Analysis of Mackenzie River Discharge and NDVI Relationship. *Can. J. Remote Sens.* **2016**, *42*, 292–306. [CrossRef]
63. NASA Earth Observatory. Available online: https://earthobservatory.nasa.gov/world-of-change/PadmaRiver (accessed on 27 March 2019).
64. Sarker, M.H.; Koudstaal, R.; Alam, M. Rivers, Chars and Char Dwellers of Bangladesh. *Int. J. River Basin Manag.* **2003**, *1*, 61–80. [CrossRef]
65. AECOM New Zealand Limited (Ed.) *Padma Multipurpose Bridge Design Project: Updated Scheme Design Report for River Training Works*; Bangladesh Bridge Authority: Dhaka, Bangladesh, 2010; Volume 1.
66. Bangladesh Water Development Board. Available online: http://www.hydrology.bwdb.gov.bd/index.php?pagetitle=discharge_data_view&sub2=139&_subid=132&id=134 (accessed on 20 March 2021).
67. Billah, M.M. Mapping and Monitoring Erosion-Accretion in an Alluvial River Using Satellite Imagery-The River Bank Changes of The Padma River in Bangladesh. *Quaestiones Geographicae* **2018**, *37*, 87–95. [CrossRef]
68. Moran, M.S.; Jackson, R.D.; Slater, P.N.; Teillet, P.M. Evaluation of Simplified Procedures for Retrieval of Land Surface Reflectance Factors from Satellite Sensor Output. *Remote Sens. Environ.* **1992**, *41*, 169–184. [CrossRef]
69. Congedo, L. Semi-Automatic Classification Plugin: A Python tool for the download and processing of remote sensing images in QGIS. *J. Open Source Softw.* **2021**, *6*, 3172. [CrossRef]
70. Gandhi, G.M.; Parthiban, S.; Thummalu, N.; Christy, A. Ndvi: Vegetation Change Detection Using Remote Sensing and Gis—A Case Study of Vellore District. *Procedia Comput. Sci.* **2015**, *57*, 1199–1210. [CrossRef]
71. Ye, S.; Reisinger, A.J.; Tank, J.L.; Baker, M.A.; Hall, R.O., Jr.; Rosi, E.J.; Sivapalan, M. Scaling Dissolved Nutrient Removal in River Networks: A Comparative Modeling Investigation. *Water Resour. Res.* **2017**, *53*, 9623–9641. [CrossRef]
72. Basu, N.B.; Rao, P.S.C.; Thompson, S.E.; Loukinova, N.V.; Donner, S.D.; Ye, S.; Sivapalan, M. Spatiotemporal Averaging of In-Stream Solute Removal Dynamics. *Water Resour. Res.* **2011**, *47*, W00J06. [CrossRef]
73. Mulholland, A.P.J.; Webster, J.R.; Mulholland, P.J.; Webster, J.R. Nutrient Dynamics in Streams and the Role of J-NABS Nutrient Dynamics in Streams and the Role of J-NABS. *J. North Am. Benthol. Soc.* **2010**, *29*, 100–117. [CrossRef]
74. Seitzinger, S.; Harrison, J.A.; Böhlke, J.K.; Bouwman, A.F.; Lowrance, R.; Peterson, B.; Tobias, C.; van Drecht, G. Denitrification across Landscapes and Waterscapes: A Synthesis. *Ecol. Appl.* **2006**, *16*, 2064–2090. [CrossRef]
75. Alexander, R.B.; Smith, R.A.; Schwarz, G.E. Effect of Stream Channel Size on the Delivery of Nitrogen to the Gulf of Mexico. *Nature* **2000**, *403*, 758–761. [CrossRef]
76. Lang, S.; Blaschke, T. *Landschaftsanalyse Mit GIS*; utb GmbH: Stuttgart, Germany, 2007; ISBN 9783838583471.
77. Venables, W.N.; Smith, D.M.; R Development Core Team. *An Introduction to R*; Notes on R: A Programming Environment for Data Analysis and Graphics; R Development Core Team: Vienna, Austria, 2021.
78. González del Tánago, M.; Martínez-Fernández, V.; Aguiar, F.C.; Bertoldi, W.; Dufour, S.; García de Jalón, D.; Garófano-Gómez, V.; Mandzukovski, D.; Rodríguez-González, P.M. Improving River Hydromorphological Assessment through Better Integration of Riparian Vegetation: Scientific Evidence and Guidelines. *J. Environ. Manag.* **2021**, *292*, 112730. [CrossRef]
79. Vaughan, I.P.; Diamond, M.; Gurnell, A.M.; Hall, K.A.; Jenkins, A.; Milner, N.J.; Naylor, L.A.; Sear, D.A.; Woodward, G.; Ormerod, S.J. Integrating Ecology with Hydromorphology: A Priority for River Science and Management. *Aquat. Conserv. Mar. Freshw. Ecosyst.* **2009**, *19*, 113–125. [CrossRef]
80. Towfiqul Islam, A.B.M. Assessment of Fluvial Channel Dynamics of Padma River in Northwestern Bangladesh. *Univers. J. Geosci.* **2016**, *4*, 41–49. [CrossRef]
81. Liu, X.; Shi, C.; Zhou, Y.; Gu, Z.; Li, H. Response of Erosion and Deposition of Channel Bed, Banks and Floodplains Towater and Sediment Changes in the Lower Yellow River, China. *Water* **2019**, *11*, 357. [CrossRef]
82. Mahmud, I.H.; Pal, P.K.; Rahman, A.; Yunus, A. A Study on Seasonal Variation of Hydrodynamic Parameters of Padma River. *J. Mod. Sci. Technol.* **2017**, *5*, 1–10.
83. Masotti, I.; Aparicio-Rizzo, P.; Yevenes, M.A.; Garreaud, R.; Belmar, L.; Farías, L. The Influence of River Discharge on Nutrient Export and Phytoplankton Biomass off the Central Chile Coast (33°–37°S): Seasonal Cycle and Interannual Variability. *Front. Mar. Sci.* **2018**, *5*, 423. [CrossRef]
84. Nawfee, S.M.; Dewan, A.; Rashid, T. Integrating Subsurface Stratigraphic Records with Satellite Images to Investigate Channel Change and Bar Evolution: A Case Study of the Padma River, Bangladesh. *Environ. Earth Sci.* **2018**, *77*, 89. [CrossRef]
85. Hossain, M.A.; Gan, T.Y.; Baki, A.B.M. Assessing Morphological Changes of the Ganges River Using Satellite Images. *Quat. Int.* **2013**, *304*, 142–155. [CrossRef]
86. Wampler, P.J. Rivers and Streams-Water and Sediment in Motion. *Nat. Educ. Knowl.* **2012**, *3*, 18.
87. Shields, F.D.; Copeland, R.R.; Klingeman, P.C.; Doyle, M.W.; Simon, A. Design for Stream Restoration. *J. Hydraul. Eng.* **2003**, *129*, 575–584. [CrossRef]

88. Knighton, A.D. *Fluvial Forms and Processes: A New Perspective*; Edward Arnold Publishers: London, UK, 1998; 383p, ISBN 0340663138. [CrossRef]
89. Pareta, K.; Pareta, U. Geomorphic Classification and Mapping of Rapti River System Using Satellite Remote Sensing Data. *Am. J. Geophys. Geochem. Geosystems* **2020**, *6*, 1–15.
90. Meshkova, L.V.; Carling, P.A. The Geomorphological Characteristics of the Mekong River in Northern Cambodia: A Mixed Bedrock–Alluvial Multi-Channel Network. *Geomorphology* **2012**, *147–148*, 2–17. [CrossRef]
91. Latrubesse, E.M. Patterns of Anabranching Channels: The Ultimate End-Member Adjustment of Mega Rivers. *Geomorphology* **2008**, *101*, 130–145. [CrossRef]
92. Palta, M.M.; Ehrenfeld, J.G.; Giménez, D.; Groffman, P.M.; Subroy, V. Soil Texture and Water Retention as Spatial Predictors of Denitrification in Urban Wetlands. *Soil Biol. Biochem.* **2016**, *101*, 237–250. [CrossRef]
93. Marton, J.M.; Creed, I.F.; Lewis, D.B.; Lane, C.R.; Basu, N.B.; Cohen, M.J.; Craft, C.B. Geographically Isolated Wetlands Are Important Biogeochemical Reactors on the Landscape. *BioScience* **2015**, *65*, 408–418. [CrossRef]
94. Pribyl, A.L.; Mccutchan, J.H.; Lewis, W.M.; Saunders, J.F., III. Whole-System Estimation of Denitrification in a Plains River: A Comparison of Two Methods. *Biogeochemistry* **2005**, *73*, 439–455. [CrossRef]
95. Wang, W.; Hu, P.; Yang, Z.; Wang, J.; Zhao, J.; Zeng, Q.; Liu, H.; Yang, Q. Prediction of NDVI Dynamics under Different Ecological Water Supplementation Scenarios Based on a Long Short-Term Memory Network in the Zhalong Wetland, China. *J. Hydrol.* **2022**, *608*, 127626. [CrossRef]
96. Liang, S.; Gong, Z.; Wang, Y.; Zhao, J.; Zhao, W. Accurate Monitoring of Submerged Aquatic Vegetation in a Macrophytic Lake Using Time-Series Sentinel-2 Images. *Remote Sens.* **2022**, *14*, 640. [CrossRef]
97. Fu, B.; Burgher, I. Riparian Vegetation NDVI Dynamics and Its Relationship with Climate, Surface Water and Groundwater. *J. Arid Environ.* **2015**, *113*, 59–68. [CrossRef]
98. Khare, S.; Deslauriers, A.; Morin, H.; Latifi, H.; Rossi, S. Comparing Time-Lapse PhenoCams with Satellite Observations across the Boreal Forest of Quebec, Canada. *Remote Sens.* **2021**, *14*, 100. [CrossRef]
99. Yu, L.; Leng, G. Identifying the Paths and Contributions of Climate Impacts on the Variation in Land Surface Albedo over the Arctic. *Agric. For. Meteorol.* **2022**, *313*, 108772. [CrossRef]
100. Munyati, C. Detecting the Distribution of Grass Aboveground Biomass on a Rangeland Using Sentinel-2 MSI Vegetation Indices. *Adv. Space Res.* **2022**, *69*, 1130–1145. [CrossRef]
101. Mia, M.B.; Hasan, T.; Akhter, S.H. Change Detection of Landuse-Landcover in and around Cox's Bazar-Teknaf Coastal Area of Bangladesh Using Satellite Images. *Dhaka Univ. J. Earth Environ. Sci.* **2019**, *8*, 1–9. [CrossRef]
102. Redhead, J.W.; May, L.; Oliver, T.H.; Hamel, P.; Sharp, R.; Bullock, J.M. National Scale Evaluation of the InVEST Nutrient Retention Model in the United Kingdom. *Sci. Total Environ.* **2018**, *610–611*, 666–677. [CrossRef]
103. Decsi, B.; Vári, Á.; Kozma, Z. The Effect of Future Land Use Changes on Hydrologic Ecosystem Services: A Case Study from the Zala Catchment, Hungary. *Biologia Futura* **2020**, *71*, 405–418. [CrossRef]
104. Piedelobo, L.; Ortega-Terol, D.; del Pozo, S.; Hernández-López, D.; Ballesteros, R.; Moreno, M.; Molina, J.-L.; González-Aguilera, D. HidroMap: A New Tool for Irrigation Monitoring and Management Using Free Satellite Imagery. *ISPRS Int. J. Geo-Inf.* **2018**, *7*, 220. [CrossRef]
105. Yousaf, A.; Khalid, N.; Aqeel, M.; Noman, A.; Naeem, N.; Sarfraz, W.; Ejaz, U.; Qaiser, Z.; Khalid, A. Nitrogen Dynamics in Wetland Systems and Its Impact on Biodiversity. *Nitrogen* **2021**, *2*, 13. [CrossRef]
106. Ma, L.; Xiong, Z.; Yao, L.; Liu, G.; Zhang, Q.; Liu, W. Soil Properties Alter Plant and Microbial Communities to Modulate Denitrification Rates in Subtropical Riparian Wetlands. *Land Degrad. Dev.* **2020**, *31*, 1792–1802. [CrossRef]
107. Kayima, J.K.; Mayo, A.W. Nitrogen Removal Buffer Capacity of the Lubigi Wetland in Uganda. *Phys. Chem. Earth Parts A/B/C* **2020**, *117*, 102883. [CrossRef]
108. Wyrick, J.R.; Senter, A.E.; Pasternack, G.B. Revealing the Natural Complexity of Fluvial Morphology through 2D Hydrodynamic Delineation of River Landforms. *Geomorphology* **2014**, *210*, 14–22. [CrossRef]